Volume 10
Number 11
1 November 2025
Pages 901–998

MSDE

Molecular Systems Design & Engineering

rsc.li/molecular-engineering

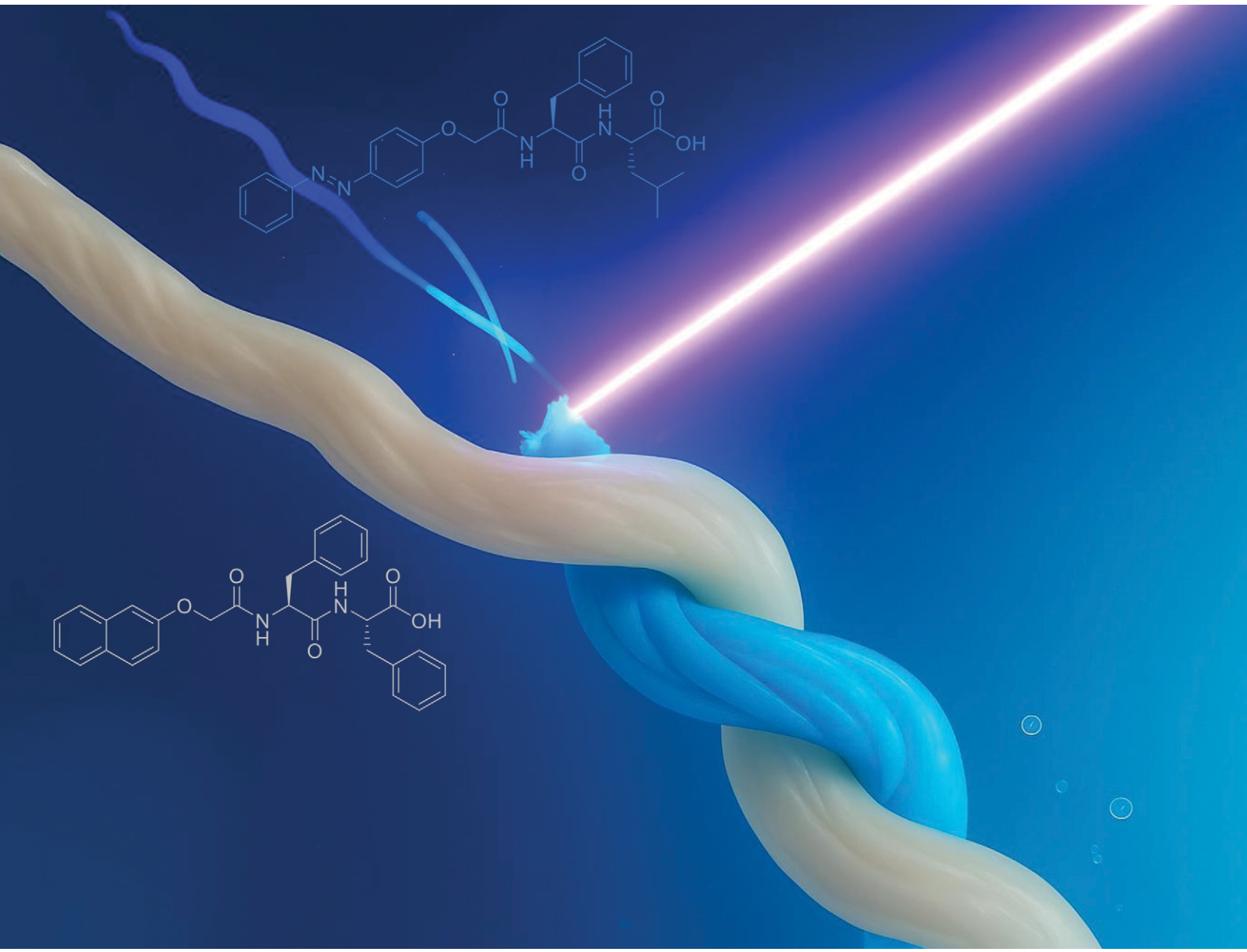

ISSN 2058-9689

ROYAL SOCIETY OF CHEMISTRY

PAPER

Massimo Vassalli, Dave J. Adams *et al.*

Probing the structure and mechanics of intertwined homo- and hetero-supramolecular gel noodles

IChemE ADVANCING CHEMICAL ENGINEERING WORLDWIDE

MSDE

PAPER

View Article Online
View Journal | View Issue

Cite this: *Mol. Syst. Des. Eng.*, 2025, **10**, 922

Probing the structure and mechanics of intertwined homo- and hetero-supramolecular gel noodles

Dipankar Ghosh, [a] Rui Huang, [a] Najet Mahmoudi, [b] Lauren Matthews, [b] Charlie Patterson,[c] Chris Holland, [d] Massimo Vassalli *[e] and Dave J. Adams *[a]

Shaping supramolecular hydrogels formed using low molecular weight gelators (LMWGs) into architecturally complex and multifunctional materials is a significant challenge. Here, we introduce a strategy to mechanically twist multiple 1D supramolecular gel filaments (gel noodles) into robust, multifunctional, and stimuli-responsive structures. Twisting introduced mechanical interlocking, which in two identical filaments yielded marginal improvement in tensile performance, while compositionally distinct gel noodles exhibited up to ~25% increase in strength due to effective load redistribution and frictional contact. However, twisting three or more filaments reduced mechanical strength, likely due to high internal strain and the formation of misaligned bundles, an effect consistent with stochastic failure propagation in twisted fibre assemblies. These results highlight the dual nature of intertwining multiple noodles: it can reinforce or compromise mechanical robustness depending on geometry and filament interactions. Despite this, twisting chemically distinct noodles enabled the formation of robust structures with spatially separated functionalities, such as photoresponsiveness, while maintaining structural integrity. This modular strategy offers a tunable platform for engineering hierarchical materials with potential for future application-specific studies.

Received 26th June 2025,
Accepted 8th September 2025

DOI: 10.1039/d5me00105f

rsc.li/molecular-engineering

Design, System, Application

Self-assembled peptides can be processed into gel noodles, with the properties of the noodles being controlled by the pre-gel solutions. These noodles are robust and can be formed in lengths of >1 m. Here we show how multiple noodles can be twisted together to form both homo and hetero-structures. This allows us to use one noodle for mechanical strength combined with one chosen for functional properties, such as photoresponsiveness. This modular strategy offers a tunable platform for engineering hierarchical materials suited for soft robotics, adaptive scaffolds, and responsive delivery systems.

Introduction

Supramolecular hydrogels with macroscopic shapes and specific structures have gained significant attention due to their unique characteristics, including internal fibrillar alignment, cross-sectional patterning, programmable shape-memory performance, and the ability to form macroscale 3D architectures.[1–6] These properties make them valuable in diverse applications such as stimuli-responsive shape deformation, tissue engineering, drug delivery, and sensing.[7–10] Recent reports demonstrate programmable supramolecular hydrogels, including chemically fuelled or logic-gated systems with timed lifecycles and multistate pathways,[11,12] and injectable depots with programmable nanoparticle release.[13] However, shaping gels formed by the self-assembly of low molecular weight gelators (LMWGs) poses considerable challenges. Unlike polymer gels, LMWGs often exhibit inferior rheological properties, resulting in fragile materials with limited mechanical robustness and structural versatility.[1] The self-assembly process is also highly sensitive to environmental conditions, making it difficult to achieve consistent and scalable morphologies.

To overcome these challenges, different strategies have been developed to control the morphologies of supramolecular gels, producing fibres, ribbons, and sheets.[14–18] Among these, one-dimensional (1D) gel filaments have emerged as a promising avenue due to their enhanced fibrillar alignment, robust yet flexible mechanical characteristics, and potential for hierarchical assembly.[19–23]

[a] *School of Chemistry, University of Glasgow, Glasgow, G12 8QQ, UK. E-mail: dave.adams@glasgow.ac.uk*
[b] *ISIS Pulsed Neutron and Muon Source, Harwell Science and Innovation Campus, Didcot, OX11 0QX, UK*
[c] *School of Engineering, University of Glasgow, Rankine Building, G12 8LT, UK*
[d] *School of Chemical, Materials and Biological Engineering, University of Sheffield, Sir Robert Hadfield Building, Mappin Street, Sheffield S1 3JD, UK*
[e] *Centre for the Cellular Microenvironment, University of Glasgow, G12 8LT, UK. E-mail: massimo.vassalli@glasgow.ac.uk*

Inspired by the pioneering work by Stupp's group on ionic cross-linking to create 1D gel filaments,[14] we introduced a method to fabricate meter-long supramolecular gel filaments, termed "gel noodles", using low molecular weight dipeptide hydrogelators and calcium chloride ($CaCl_2$).[22] These gel noodles are biocompatible with tunable physical properties, and can be functionalised at the N-terminal, offering exceptional versatility for applications.[14,24–27]

Despite their advantages, gel noodles remain limited by their one-dimensionality, restricted functionality, and the inability of some materials to form mechanically robust yet flexible filaments. To address these limitations, we introduce twisting as a strategy to transform individual gel noodles into next-generation supramolecular materials. By twisting multiple 1D filaments with distinct functionalities or mechanical properties, we can create intertwined gel noodles that combine the strengths of their individual components. For instance, twisting a functional but mechanically weak noodle with a mechanically stable one yields a robust yet functional material. Moreover, these twisted structures can serve as macroscopically separated self-sorted systems, providing new opportunities for multifunctionality and stimuli responsiveness.

Twisting or weaving as a concept has long been used in textile fibre engineering or when fabricating artificial muscles to create robust and functional materials with tailored mechanical and functional properties.[28–31] While intertwining pre-existing fibres within a gel to create distinct hierarchical networks,[32,33] fabricating core-shell structures,[34] as well as layering or stacking macroscopic gels has been extensively used to develop multilayer or gradient hydrogels,[35–37] our work goes beyond these approaches by utilizing 1D gel filaments to construct finely twisted assemblies with enhanced structural complexity. These structures are designed to provide enhanced mechanical strength and flexibility while incorporating multifunctional properties.[38,39]

Here, we demonstrate twisting of long 1D supramolecular gel noodles into durable, rope-like structures. Using N-functionalised dipeptide gelators,[40] we integrate distinct functionalities into the gel noodles, enabling the assembly of multifunctional materials responsive to external stimuli. This method not only addresses the limitations of traditional 1D filaments but also provides a potentially scalable approach for creating resilient, hierarchical materials. By bridging supramolecular chemistry and materials science, our strategy opens new avenues for research in biomaterials and adaptive systems, positioning gel noodles as a versatile and innovative class of soft materials.

Results and discussion

We prepared gel noodles from a number of different functionalised dipeptides such as 2NapFF, 4BPFF, 1PyrFF, and AzoFL (Fig. 1a, b and S1–S13) following a previously reported method.[22,27,41] To form robust noodles, we optimised the preparation of the precursor solutions, for example by using thermal annealing where necessary (Fig. S14–S18). The noodles formed from 2NapFF are robust and have good force and strain resistance. In comparison, those formed from 4BPFF, 1PyrFF and AzoFL are all significantly less robust. The 2NapFF and 4BPFF noodles also had slightly larger diameters (Fig. S19), likely due to the higher viscosity of their pre-gel solutions. We assessed the structural features of the gel noodles using SANS (Fig. 1c). The scattering profiles were consistent with those of the corresponding pre-gel solutions (see Fig. S15, Tables S1 and S2), suggesting that the micellar structures were preserved upon gel formation. However, the fitted micelle lengths increased substantially in the noodles, exceeding the measurable range within the SANS experiment (Tables S1 and S2). This observation supports the formation of extended, rigid structures upon Ca^{2+} crosslinking, contributing to the stabilisation of the gel noodles.

The development of functionalised noodles sets the stage for creating complex systems by combining multiple noodles. This process is challenging, as the low tensile strength of the gel filaments often leads to structural breakage during manipulation. While it is relatively easy to join two filaments side-by-side by pulling them together from an aqueous bath due to the adhesive nature of the noodles, these structures readily separate when re-immersed in water, limiting their practical use (Fig. 2a and b). To address this, we introduced a twisting technique as our noodles, especially 2NapFF, showed sufficient tensile integrity. While 2NapFF noodles are well known for their force and strain resistance,[41] the lack of active functional groups limits their use as passive matrices. 1PyrFF and 4BPFF noodles are expected to show fluorescence and UV activity, but their mechanical strength is weaker. Therefore, we hypothesised these two types of noodles could be combined *via* twisting and that would retain the functional properties of 1PyrFF, 4BPFF, or AzoFL, while 2NapFF should provide mechanical strength.

We explored the feasibility of twisting gel noodles using 2NapFF, chosen for its superior tensile strength compared to the other formulations. The twisting process was carried out using custom 3D-printed holders, with each noodle secured between two vertically placed holders. The top holder was fixed in place using a clamp and the bottom one connected to a rotating motor (Fig. 2c). After securing both ends of the noodles, the gap between the two holders was reduced by 0.5 mm by placing a 0.5 mm thick plastic spacer beneath the motor. This adjustment helped relieve tension generated during twisting, thereby minimizing the risk of filament breakage. Rotating the motor at 10 rpm resulted in intertwining of the filaments, with each full rotation introducing two crossover points. This setup provided control over the number of twists between the noodles, ensuring consistent and reproducible intertwining. The number of noodles involved in the twisting process could be adjusted by using holders with different symmetries. For example, twisting two, three, or four noodles was achieved using C_2-, C_3-, and C_4-symmetric holders, respectively (Fig. 2c–e).

For visual clarity, the 2NapFF noodles were stained with Congo red or bromocresol green, resulting in intensely red or

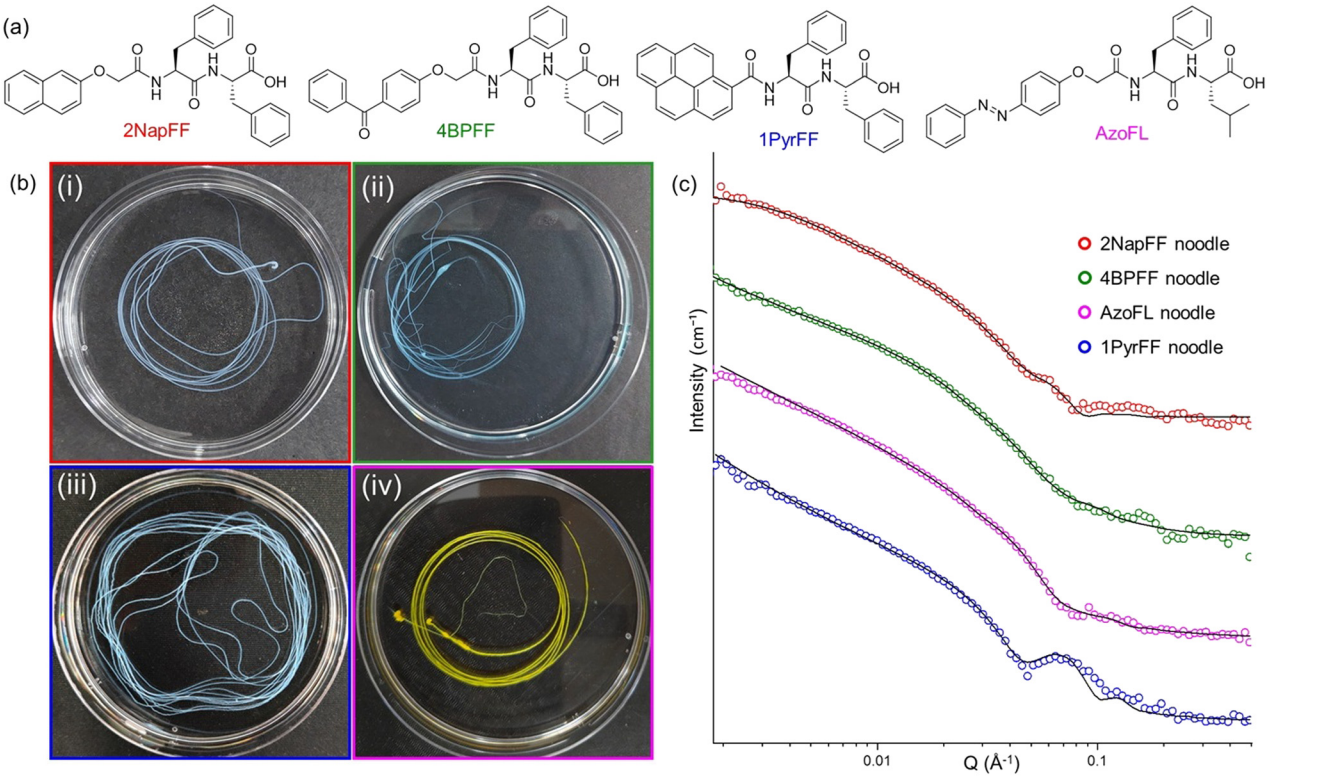

Fig. 1 (a) Chemical structures of 2NapFF, 4BPFF, 1PyrFF, and AzoFL; (b) gel noodles formed from (i) 2NapFF, (ii) 4BPFF, (iii) 1PyrFF, and (iv) AzoFL in all cases crosslinked with $CaCl_2$; (c) SANS of the gel noodles formed from 2NapFF, 4BPFF, AzoFL, and 1PyrFF solutions with 0.5 M $CaCl_2$. The data are shown as empty circles and the fits as black lines (full fit parameters are listed in Table S2). The data are offset on the intensity scale for ease of discrimination and the error bars are omitted for clarity.

pale blue noodles. Intertwining two strands of 2NapFF resulted in a rope-like filament, where the length of two consecutive crossover points (formed by 360° rotation or one full twist) ranged from 4 to 5 mm (Fig. 2c). The spacing between crossovers was not perfectly uniform along the twisted noodle. Small variations arose from factors such as the total noodle length and slight offsets of each strand relative to the rotation axis. The crossover spacing was slightly shorter on the side where the rotating motor was attached compared to the static end. Since mounting and alignment were performed manually, these parameters could not be held constant from run to run, but any introduced variation is expected to be consistent across all sample groups tested. This protocol was then extended to fabricate twisted constructs using three or four noodles (Fig. 2d and e). We also demonstrated hetero-twisting by pairing 2NapFF with functional but mechanically weaker noodles such as 4BPFF, 1PyrFF, and AzoFL (Fig. S20). This design strategy enabled the integration of distinct functionalities into robust macroscopic structures.

To understand the mechanical deformation involved in the twisting process, we studied force measurements during twisting using a tensile tester. The setup was designed by mounting two 2NapFF noodles (AB and A′B′, Fig. 3) onto two C_2-symmetric holders with a grip-to-grip distance of 40.5 mm. The top holder, securing the A and A′ ends of the noodles, was fixed in place, while the lower holder, attached to the B and B′ ends, was connected to a rotating motor (Fig. S21). Before initiating the twisting process, the gap between the holders was reduced by 0.5 mm to relieve residual tension (resulting a grip-to-grip distance of 40 mm), thereby minimizing the risk of filament breakage during twisting. The motor was rotated at 10 rpm, and the tensile force was continuously recorded over time as twisting proceeded. Tensile force profiles from five independent experiments using two 2NapFF noodles are shown in Fig. S22, while the average force response during twisting is presented in Fig. 3. The force profile exhibited periodic fluctuations corresponding to each full rotation. The tensile force increased with each twist, reflecting the buildup of internal stress. A peak in tensile force was typically observed at 180° rotation, followed by relaxation as the twist completed. As twisting continued, the force progressively rose, reflecting the growing mechanical load from successive twists. Eventually, the force plateaued, indicating structural adaptation, until a sudden drop marked the breaking point of one noodle. The average force recorded at this point was approximately 6 mN, representing the total load shared by both noodles (Fig. 3). This threshold provides a benchmark for the minimum tensile strength required for noodles to be successfully twisted without breakage. Weaker formulations that cannot tolerate this force are prone to failure during the twisting process and thus unsuitable for stable intertwined architectures.

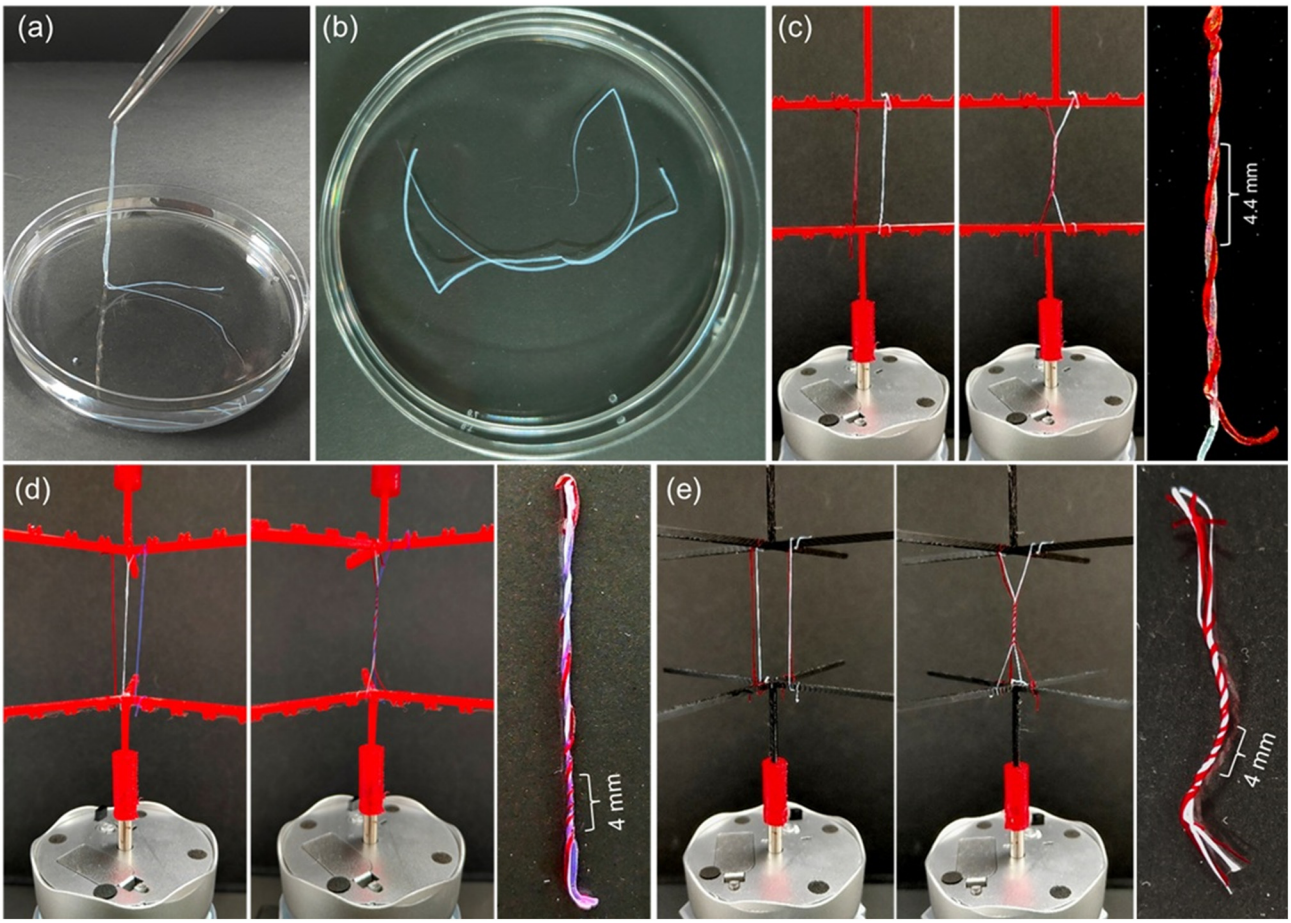

Fig. 2 (a) Joining two 2NapFF noodles side-by-side, (b) separation of the noodles in water. (c–e) Twisting two, three, and four 2NapFF noodles using a rotating motor (at bottom end): before twisting (left), after 5 twists (middle), and the resulting twisted noodle (right). The red and blue noodles are stained with Congo red and bromocresol green for distinction. The grip-to-grip distance is 40.5 mm before twisting and 40 mm after twisting.

Next, we evaluated how twisting influenced the tensile performance of the gel noodles. The twisted noodles were prepared as described before, but unstained noodles were used in all the experiments to avoid potential changes in mechanical properties caused by dye incorporation (Fig. S23–S26). Individual 2NapFF noodles exhibited tensile strengths in the range of 4–5 mN (Fig. S27 and Table S3). Mounting two noodles in parallel at a distance did not result in significant additive mechanical strength (Fig. S28). Instead, the filaments typically failed sequentially—one breaking before the other—resulting in only modest gains in most cases. Lateral adhesion between two noodles, facilitated by surface tackiness, resulted in stronger constructs; however, the ultimate force at rupture remained less than twice that of an individual 2NapFF noodle (Fig. S29). This sub-additive mechanical response likely arises from uneven load distribution and the absence of effective mechanical interlocking, which causes one filament to bear more stress than the other.[42] Once the weaker noodle fails, the overall structure destabilizes, leading to premature rupture before full load transfer can occur. To assess the effect of mechanical interlocking, we twisted two noodles together by 5, 10, or 15 full rotations (creating 10, 20, and 30 crossover points, respectively) over a 6 cm length (Fig. S23 and S24). The twisted constructs exhibited slightly improved tensile strength and strain tolerance relative to their untwisted counterparts (Fig. 4a and S30–S32). Statistical analysis *via* two-sample t-tests showed no significant differences in either peak force or strain at break across the twisted and untwisted samples ($p > 0.05$ in all cases). However, the observed trend indicating a modest improvement in ultimate force for the twisted constructs suggests that mechanical interlocking may reduce localised stress concentration.[43,44] By physically entangling the filaments, the twisted geometry could promote partial redistribution of mechanical load during elongation. Furthermore, the twisted configuration might act as a structural buffer, accommodating small deformations before full tension is transmitted along the filaments. The increase in strain capacity at higher twist levels (15 rotations) can be attributed to uncoiling of helical structures during elongation.

To investigate scalability and structural complexity, we extended our tensile analysis to three- and four-strand assemblies (Fig. S25 and S26). Similar to the two-strand

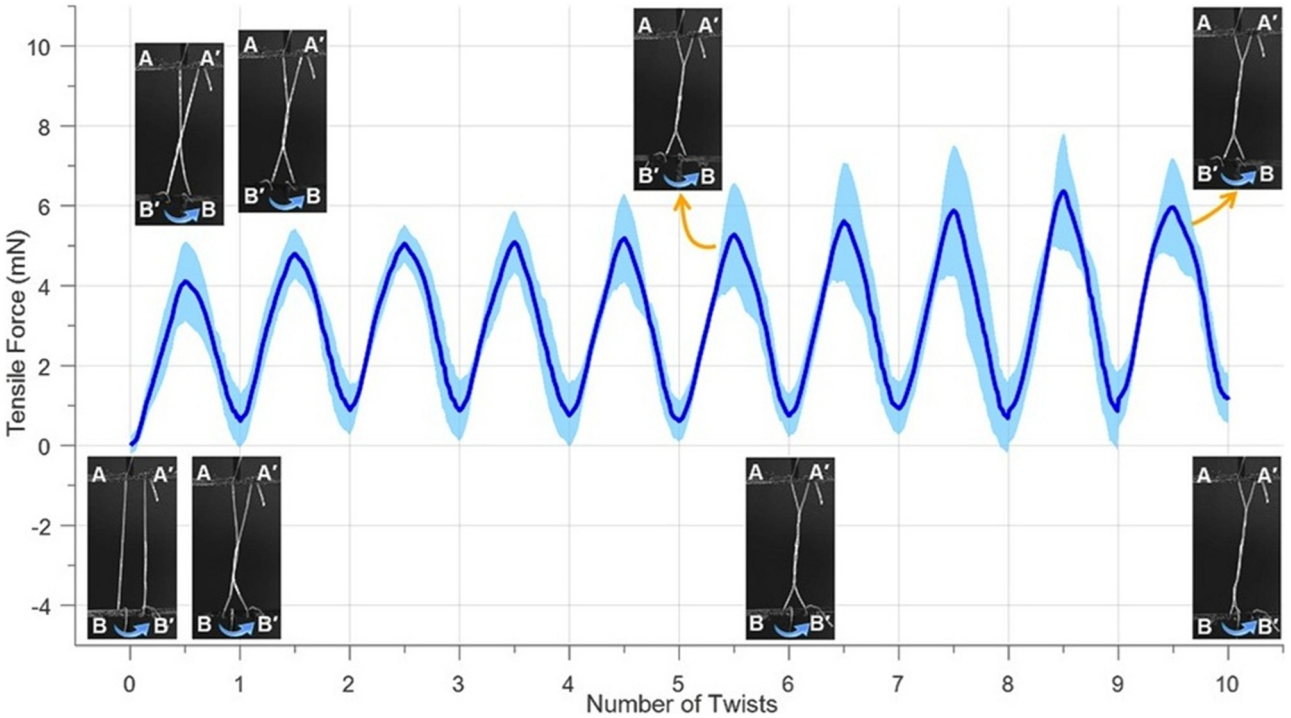

Fig. 3 Periodic fluctuations in tensile force during the twisting of two 2NapFF noodles. The blue line represents the average force response from five independent experiments, and the shaded cyan region indicates the standard deviation. Inset images show representative frames from one experiment illustrating the twisting process.

system, untwisted bundles showed increased tensile forces with filament number, but the performance did not scale linearly (Fig. 4b, S33 and S34), suggesting uneven load distribution and premature failure triggered by the weakest component.[42,45] Interestingly, twisted constructs of three and four noodles (with 10 full rotations over 6 cm) showed a decrease in ultimate tensile force compared to the untwisted counterparts (Fig. 4b, S35 and S36). This result suggests a possible contribution from stress localization and internal strain in the ground state (before applying any external deformation), which may arise during the twisting of multi-filament systems.[43,46,47] Such effects may reduce the effective fibre alignment along the load direction and, in turn, decrease mechanical robustness.[48] Thus, while intertwining improves the strength of two-strand systems, its effectiveness decreases as more filaments are added.

Finally, we assessed the mechanical behaviour of hetero-noodle systems, combining 2NapFF with either 1PyrFF or 4BPFF (Fig. 4c). Individually, 1PyrFF and 4BPFF noodles exhibited lower tensile strengths, ~60–75% of that of 2NapFF (Fig. S37 and S38). When paired laterally without twisting, the composite strength exceeded the sum of the individual noodle strengths, with an increase of around 10% (Fig. S39 and S40). This modest enhancement may arise from frictional contact and minor cooperative load-bearing.[49,50] Upon twisting (10 full rotations over 6 cm), the tensile strength further improved by ~20–25% relative to the sum of individual strengths (Fig. S41, S42 and Table S3). This significant improvement suggests that enhanced physical integration, such as frictional forces between the hetero-noodles, and possible inter-filament interactions may improve load transfer and cohesion in these heterostructures.[49,51] The results demonstrate a viable strategy for reinforcing functional but mechanically weaker filaments through intertwining with stronger noodles, an important step toward robust, multifunctional supramolecular architectures.

Comparison of the force-strain profiles of twisted and untwisted gel noodles revealed that twisting can either enhance or reduce tensile resistance, depending on the configuration. This duality is expected, as twisting introduces opposing effects that can both strengthen or weaken the structure. For example, improved load redistribution *via* filament interlocking, increased lateral pressure and friction, enhanced inter-strand crosslinking, and a transition to a quasibrittle failure mode arising from slight filament misalignments can increase the ultimate force tolerance.[44,50,51] On the other hand, twisting can induce fibre misalignment, surface damage, pre-shear defects, and premature failure initiated at the weakest strand, all of which compromise tensile strength.[46,47,52] Thus, the mechanical robustness of twisted assemblies critically depends on the choice of gelators, the twisting protocol, and the degree of intertwining.

Although the twisted 2NapFF noodles demonstrated comparable (in two-strand systems) or reduced (in three- and four-strand systems) force resistance relative to untwisted assemblies, they exhibited significant internal deformation

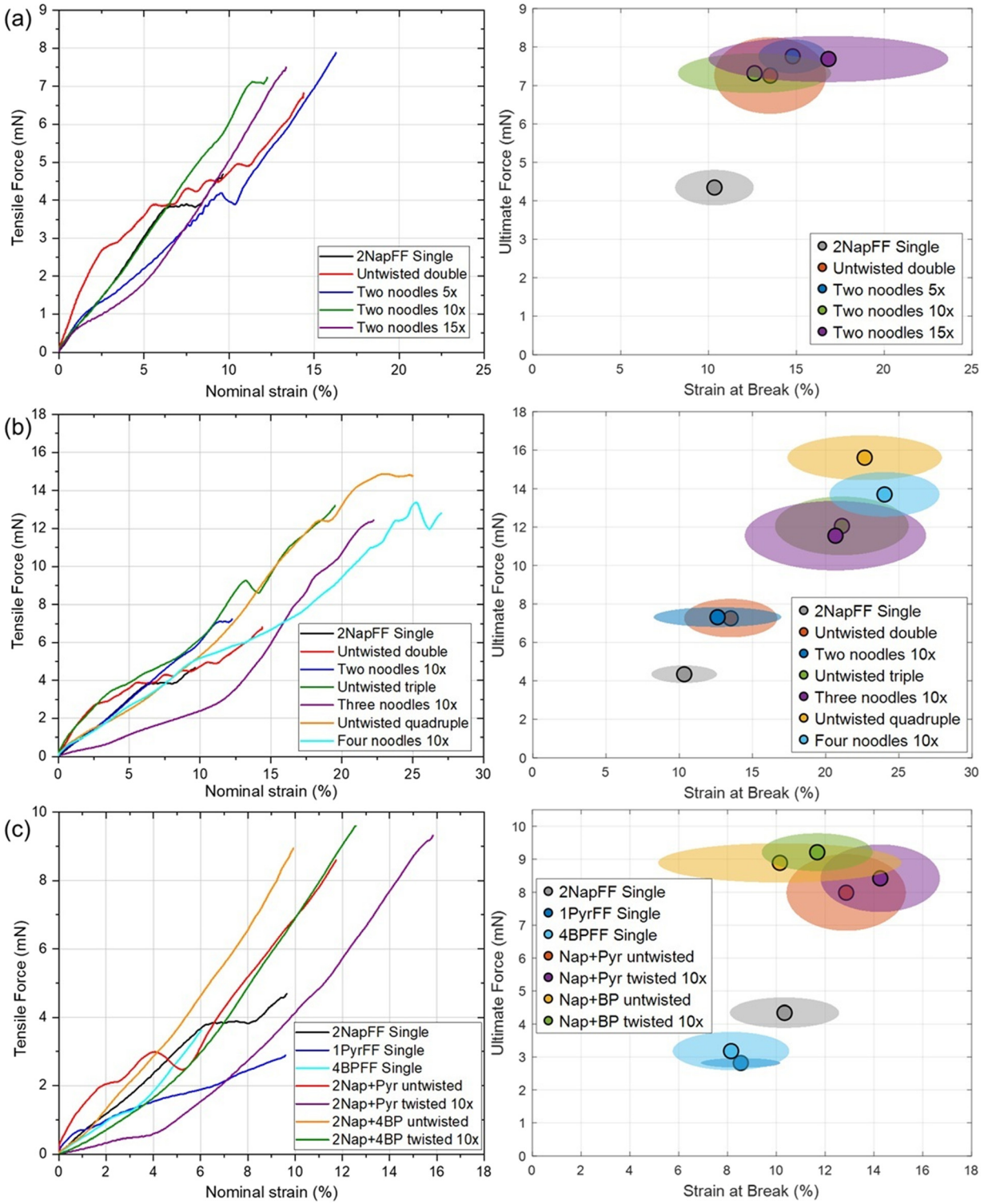

Fig. 4 Comparison of the ultimate tensile force and strain at break for various gel noodles: (a) 2NapFF single, untwisted double, and two noodles twisted with 5×, 10×, and 15× rotations; (b) two, three, and four 2NapFF noodles; (c) 2NapFF noodles untwisted and twisted with 1PyrFF and 4BPFF. In each panel, the left plot shows one representative force–strain curve for visual comparison. The right plot shows the distribution of results across five independent repeats for each sample. Data points represent the mean strain and force at break, and the shaded ellipses indicate the spread corresponding to the standard deviation in both force and strain dimensions. The individual values of the ultimate force and strain at break, along with their averages and standard deviations, are listed in Table S3.

(Fig. 3). This pre-strain suggests that twisted noodles do not begin tensile extension from a relaxed, zero-stress state. As shown in Fig. 3, a two-noodle twisted system typically stores ~1–2 mN of internal force prior to stretching, while three-

Table 1 Maximum slopes of the force-strain curves for 2NapFF gel noodles, calculated from segmental analysis using 0.5% strain intervals

Noodle	Force-strain $Slope_{max}$	Relative ratio
2NapFF single	0.80 ± 0.14	1
Untwisted 2×	1.15 ± 0.47	1.43
Twisted 2×	1.25 ± 0.74	1.56
Untwisted 3×	1.72 ± 0.51	2.15
Twisted 3×	1.22 ± 0.10	1.51
Untwisted 4×	1.30 ± 0.18	1.61
Twisted 4×	1.63 ± 0.58	2.03

and four-strand configurations likely accumulate even greater baseline forces due to increased filament overlap and higher initial deformation. To directly compare the mechanical behaviour of twisted and untwisted noodles from an equivalent starting point, we attempted to perform sequential twisting and tensile testing within a single experimental run. However, these trials were unsuccessful as post-twisting, tensile loading consistently led to rupture at one of the individual strands rather than within the twisted region (Fig. S43). Thus, these tests did not accurately reflect the tensile behaviour of the integrated twisted construct.

We further assessed the relative elasticity of the 2NapFF noodles by comparing the force-strain slopes. Table 1 summarises the average maximum slopes for each assembly, along with their relative ratios normalised to the single noodle. These data highlight the variability in mechanical responses across different configurations. Constructs with a greater number of filaments generally exhibited higher maximum slopes, indicating enhanced stiffness.

The mechanical properties of the twisted noodles suggest that a fragile noodle can benefit from structural support provided by a more robust counterpart through intertwining. To validate the retention of functional properties in the twisted constructs, we analysed systems combining 2NapFF with photofunctional gelators. Twisted 2NapFF + 1PyrFF noodles appeared visibly bright under UV light, similar to the 1PyrFF noodles alone, and this strong UV visibility suggests retention of the pyrene moiety's characteristic absorption behaviour after intertwining (Fig. 5a). Similarly, the azobenzene moiety is known to undergo *cis–trans* isomerization in response to UV light, which could potentially disrupt the 1D filament structure by altering the supramolecular assembly.[53] To test this, we prepared twisted noodles by combining 2NapFF and AzoFL, then exposed them to 365 nm UV light while immersed in water to prevent drying. After 45 minutes, we observed that the AzoFL filament had broken into two fragments, whereas the 2NapFF filament remained intact (Fig. 5b). This selective degradation, dictated by the chemical composition of the individual noodles, adds additional functionality to the system, making it adaptable for a wide range of stimuli-responsive applications.[54] Overall, these results show that twisting is a useful way to create strong and multifunctional supramolecular gel structures. By combining robust gelators with more fragile but functional ones, we can make stable materials that retain their special properties. This modular approach also allows us to keep different functions in separate segments of the structure. As a result, this method offers new possibilities for designing soft materials that can respond to stimuli, change shape, and maintain tensile integrity under load.

Conclusions

In this study, we demonstrate the design and fabrication of twisted supramolecular gel noodles as a versatile approach to engineer hierarchical, mechanically tunable, and functionally diverse soft materials. By optimising pre-gel conditions, including concentration and thermal annealing, we generated stable 1D gel filaments from functional gelators

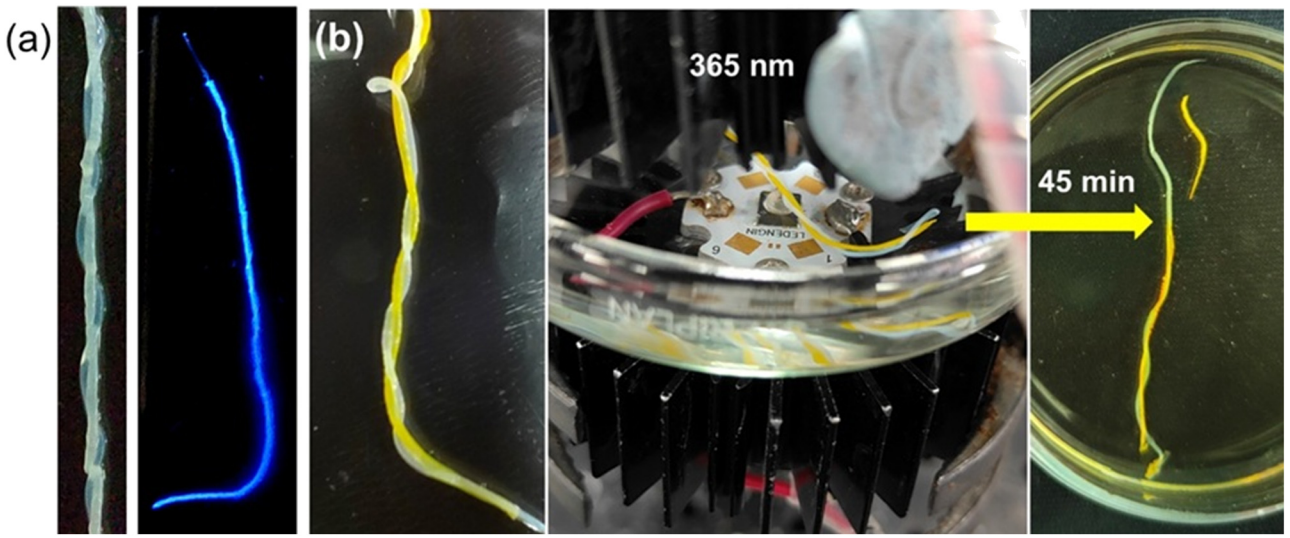

Fig. 5 (a) 2NapFF and 1PyrFF twisted noodle under visible and UV-light. (b) Selective collapse of AzoFL noodle from the twisted 2NapFF + AzoFL noodle by UV light.

such as 1PyrFF, 4BPFF, and AzoFL. These noodles were mechanically inferior to 2NapFF noodles but possess desirable properties like UV responsiveness or photodegradability. Using customised setup, we twisted filaments to form complex structures, with tensile measurements showing that an approximate force threshold of 6 mN was needed for successful twisting. Two-strand twisted noodles exhibited improved tensile strength compared to the non-twisted ones due to mechanical interlocking, while higher-order twisting (three- and four-strand) showed reduced strength, likely due to stress localization and internal strain. Hetero-twisting 2NapFF with functional noodles significantly enhanced mechanical integrity (by ~25%) while preserving functionality, as evidenced by selective photodegradation of AzoFL noodle. These intertwining architectures allow us to combine the mechanical strength and functional properties of different filaments, enabling independent control over structure and function within a single material. This approach offers new possibilities to create adaptive biomaterials, soft robotics, and programmable delivery systems where resilience and multifunctionality are essential.

Experimental

Materials and methods

All chemicals were purchased from Sigma-Aldrich or Fluorochem Ltd and used as received. Deionised water was used in all experiments. The detailed synthetic procedures are provided in the SI.

Preparation of the dipeptide solutions

2NapFF solution was prepared by stirring 400 mg (0.806 mmol) of 2NapFF, 11.94 mL of deionised water, and 8.06 mL of 0.1 M NaOH. This blend was stirred continuously for approximately 20 hours at ambient temperature (around 20 °C) using a 25 × 8 mm stirrer bar within a 50 mL centrifuge tube at a speed of 750 rpm. The pH of the resulting solution was adjusted to 10.5 ± 0.05 using 1.0 M NaOH.

Similarly, 1PyrFF and AzoFL solutions were prepared by mixing 200 mg of the materials with 1 equivalent of NaOH (0.1 M solution) in a 14 mL glass vial, followed by adding required amount of water to attain a final volume of 5 mL. The mixtures were stirred overnight, and pH of the solutions was adjusted with 1.0 M NaOH solution. To thermally anneal the sample, the vial was then placed in an oven at 60 °C for 1 h. The vial was wrapped with Al-foil to prevent water evaporation. After 1 h, the vial was kept at room temperature for cooling. If needed, the pH was readjusted to 10.5 ± 0.05 with 1.0 M NaOH solution.

Viscosity measurements

Viscosity measurements were performed on an Anton Paar Physica MCR 101 rheometer using a 50 mm diameter, 1° cone-plate geometry (CP50) at 25 °C. The instrument-defined truncation gap was 0.101 mm. ~1 mL of the samples was poured onto the plate to avoid any shearing caused by pipetting the solutions. All viscosity measurements were carried out in triplicates, and the mean values and standard deviations were reported.

Microscopic images

Microscopic images were captured using a Leica DM750 microscope set to 5× magnification. For high pH solutions, a drop of the peptide solutions was placed on a glass slide. For noodles, about 3–4 cm length was cut from the middle segment. Initially, the white light was calibrated and brightfield images were captured. Then the polarised light was turned on and the orientation of the polariser was adjusted to 90° to capture polarised light images. The scale bars were inserted using ImageJ software v1.54h (National Institutes of Health, Maryland, USA).[55] For diameter analysis, five independent noodles per composition were imaged in brightfield. For each image, the diameter was measured at five evenly spaced locations, and the mean ± SD across all five noodles for each composition was reported.

Preparation of gel noodles

20 mL of 0.5 M freshly prepared $CaCl_2$ solution was poured into a petri dish (90 mm diameter) and rotated on a spin-coater at a speed of 100 rpm. The peptide solutions were extruded using a ProSense syringe pump, fitted with a 10 mL syringe and a 21 gauge needle, at a flow rate of 3 mL min^{-1}.

Small angle neutron scattering (SANS)

For the SANS experiments, the dipeptide pre-gel solutions and 0.5 M $CaCl_2$ solution were prepared in NaOD/D_2O medium as described above. The 1PyrFF solutions were loaded into a Hellma cuvette with a 2 mm path length. For the noodle samples, a thin sheet of Al-foil was cut and folded into a zig-zag pattern. About 2 cm segment of the noodle was then cut and positioned along the length of the folded Al-foil, with a total of 5–6 filaments placed within the foil. The prepared foil was carefully inserted into the Hellma cuvette (2 mm path length), which was then filled with D_2O and sealed. SANS experiments were carried out on the SANS2d instrument at the ISIS Neutron and Muon source (STFC Rutherford Appleton Laboratory, Didcot, UK) with a source-to-sample and sample-to-detector distance = 12 m, and neutrons of wavelength range 1.75–12.5 Å to access the Q range from 0.00154 to 0.49 $Å^{-1}$. The resulting data were converted to 1D scattering curves (intensity *vs.* Q) using Mantid data reduction software.[56] This process included subtracting the electronic background, normalizing the full detector images, and removing scattering from both the empty cell and D_2O. The instrument-agnostic data were then analysed using the SasView software v.5.0.6,[57] fitting them to the models discussed in the text.

Twisting gel noodles

Intertwined gel noodle constructs were prepared with freshly prepared noodles using two vertically aligned 3D-printed holders positioned at a specific distance (*e.g.*, 40.5 or 60.5 mm apart). The upper holder was fixed using a clamp, while the lower holder was attached to a rotating motor. Individual gel noodles (~80 mm in length for the 60.5 mm gap) were cut using scissors and mounted by securing one end to the stationary holder and the other to the rotating one. After all noodles were positioned, the gap between the holders was reduced by 0.5 mm through the insertion of a plastic spacer beneath the motor base. This adjustment relieved residual tension, minimizing the risk of filament breakage during twisting. Controlled intertwining was achieved by rotating the motor at 10 rpm, where each full rotation introduced one helical twist (two crossover points) along the noodle assembly. C_2, C_3, and C_4-symmetric holders enabled the fabrication of constructs composed of two, three, or four noodles, respectively, ensuring consistent twist density and reproducible filament alignment.

Tensile force response during twisting

The tensile force response study during twisting noodles was performed using a Zwick Z2.0 UTM testing machine (Zwick GmbH & Co. KG, Germany), controlled by TestExpert V1.8 software, and equipped with a 5 N load cell (on top). A rotating motor was fitted at the base. Two 3D-printed holders with two arms (C_2 symmetric) were attached at both ends, with a grip-to-grip distance of 40.5 mm. A segment of 6–7 cm was cut from the noodle using scissors, removed from the aqueous bath, and quickly twined around the 3D-printed grip holders. The grip-to-grip distance was then reduced to 40 mm. The rotating motor was then activated at 10 rotations per minute, causing the bottom part of the noodle to rotate. Each complete rotation resulted in one full twist (two crossover points) of the noodle. The force experienced with the rotation was recorded until either strand of the noodle was broken. Mechanical testing was performed at ambient laboratory temperature and relative humidity, and each experiment lasted less than 5 min. Under these conditions, the noodles did not dry appreciably, and their tensile properties were not affected.

Tensile testing experiments

The tensile properties of the noodles were investigated using the same Zwick machine used in the twisting-force study. After twisting the noodles, a predetermined number of times (5, 10, or 15 full rotations), they were mounted onto a custom 3D-printed grip with a 20 mm separation, ensuring that the twisted segment spanned the entire gap, and then subjected to uniaxial stretching at a rate of 5 mm min^{-1}. The applied force and strain were recorded until the noodle ruptured. The tensile strength of a single-strand filament; and two, three, and four noodles joined side-by-side (non-twisted) were also studied. For these experiments, the noodles were simply twined around the 3D-printed grip holders separated by 20 mm and stretched at 5 mm min^{-1} until rupture.

Collapsing AzoFL noodle

An AzoFL noodle was twisted with a 2NapFF noodle and immersed in water inside a petri dish. Two UV lamps (wavelength: 365 nm) were positioned at 2 cm distance from the noodle, one on the top and one on the bottom. The UV light was irradiated inside a black box, and the sample was monitored every 10 minutes until the AzoFL noodle was completely broken.

Author contributions

Conceptualization: D. G., M. V., D. J. A.; methodology: D. G., N. M., L. M., C. P., M. V., D. J. A.; data curation: D. G., R. H.; validation: D. G., C. H., M. V., D. J. A.; formal analysis: D. G., C. H., M. V., D. J. A.; investigation: D. G., C. H., M. V., D. J. A.; funding acquisition: M. V., D. J. A.; project administration: M. V., D. J. A.; resources: M. V., D. J. A.; software: D. G., N. M., L. M., C. P., supervision: M. V., D. J. A.; visualization: D. G., M. V., D. J. A.; writing – original draft: D. G., writing – review & editing: All.

Conflicts of interest

There are no conflicts to declare.

Data availability

Supplementary information: The full synthesis and characterisation of 1PyrFF and AzoFL, the optimisation of noodle preparation, additional viscosity, microscopy, and SANS data, and complete tensile force-strain datasets with summary statistics are provided in SI. See DOI: **https://doi.org/10.1039/D5ME00105F**.

The data that support the findings of this study are available from the corresponding author, Dave J. Adams (E-mail: dave.adams@glasgow.ac.uk), upon reasonable request.

Acknowledgements

We thank the Leverhulme Trust for funding (Grant code: RPG-2022-324), and Dr. Alex Loch for providing the 4BPFF compound. We thank the ISIS Neutron and Muon Source (Science and Technology Facilities Council, Rutherford Appleton Laboratory, Oxfordshire, UK) for the SANS2d beam time allocated under the experiment numbers RB2410140 (DOI: **https://doi.org/10.5286/ISIS.E.RB2410140**) and RB2420071 (DOI: **https://doi.org/10.5286/ISIS.E.RB2420071**). This work was benefitted from the SasView software, originally developed by the DANSE project under NSF award DMR-0520547.

References

1 P. R. A. Chivers and D. K. Smith, *Nat. Rev. Mater.*, 2019, **4**, 463–478.

2 X. Le, W. Lu, J. Zheng, D. Tong, N. Zhao, C. Ma, H. Xiao, J. Zhang, Y. Huang and T. Chen, *Chem. Sci.*, 2016, **7**, 6715–6720.
3 S.-J. Jeon, A. W. Hauser and R. C. Hayward, *Acc. Chem. Res.*, 2017, **50**, 161–169.
4 B. Wu, Y. Jian, X. Le, H. Lin, S. Wei, W. Lu, J. Zhang, A. Zhang, C.-F. Huang and T. Chen, *ACS Appl. Mater. Interfaces*, 2019, **11**, 48564–48573.
5 S. Bai, H. Wang, G. Gu, J. Zhang, L. Wei, Y. Gao, Z. Li, X. Guo and Y. Wang, *ACS Mater. Lett.*, 2023, **5**, 2377–2383.
6 M. Lovrak, W. E. J. Hendriksen, C. Maity, S. Mytnyk, V. van Steijn, R. Eelkema and J. H. van Esch, *Nat. Commun.*, 2017, **8**, 15317.
7 C. C. Piras, C. S. Mahon, P. G. Genever and D. K. Smith, *ACS Biomater. Sci. Eng.*, 2022, **8**, 1829–1840.
8 A. Vidyasagar, K. Handore and K. M. Sureshan, *Angew. Chem., Int. Ed.*, 2011, **50**, 8021–8024.
9 H. Wang, L. Chen, L. Fang, L. Li, J. Fang, C. Lu and Z. Xu, *Mater. Des.*, 2018, **160**, 194–202.
10 Y. Xu, D. Kraemer, B. Song, Z. Jiang, J. Zhou, J. Loomis, J. Wang, M. Li, H. Ghasemi and X. Huang, *Nat. Commun.*, 2019, **10**, 1771.
11 X. Fan and A. Walther, *Angew. Chem., Int. Ed.*, 2021, **60**, 11398–11405.
12 Z. Wang, T. Zhao, S. Yang, Y. Meng and X. Wang, *CCS Chem.*, 2024, **6**, 1951–1964.
13 W. Shi, X. Ying, X. Sheng, S. Das, D. He, K. Collins, Y. Hu and M. G. Finn, *Adv. Funct. Mater.*, 2025, **35**, 2409796.
14 S. Zhang, M. A. Greenfield, A. Mata, L. C. Palmer, R. Bitton, J. R. Mantei, C. Aparicio, M. O. de la Cruz and S. I. Stupp, *Nat. Mater.*, 2010, **9**, 594–601.
15 T. Christoff-Tempesta, Y. Cho, D.-Y. Kim, M. Geri, G. Lamour, A. J. Lew, X. Zuo, W. R. Lindemann and J. H. Ortony, *Nat. Nanotechnol.*, 2021, **16**, 447–454.
16 S. Zhang, X. Liu, S. F. Barreto-Ortiz, Y. Yu, B. P. Ginn, N. A. DeSantis, D. L. Hutton, W. L. Grayson, F.-Z. Cui, B. A. Korgel, S. Gerecht and H.-Q. Mao, *Biomaterials*, 2014, **35**, 3243–3251.
17 F. K.-C. Leung, T. Kajitani, M. C. A. Stuart, T. Fukushima and B. L. Feringa, *Angew. Chem., Int. Ed.*, 2019, **58**, 10985–10989.
18 A. B. Marciel, M. Tanyeri, B. D. Wall, J. D. Tovar, C. M. Schroeder and W. L. Wilson, *Adv. Mater.*, 2013, **25**, 6398–6404.
19 D. Kiriya, M. Ikeda, H. Onoe, M. Takinoue, H. Komatsu, Y. Shimoyama, I. Hamachi and S. Takeuchi, *Angew. Chem., Int. Ed.*, 2012, **51**, 1553–1557.
20 B. D. Wall, S. R. Diegelmann, S. Zhang, T. J. Dawidczyk, W. L. Wilson, H. E. Katz, H.-Q. Mao and J. D. Tovar, *Adv. Mater.*, 2011, **23**, 5009–5014.
21 S. R. Diegelmann, N. Hartman, N. Markovic and J. D. Tovar, *J. Am. Chem. Soc.*, 2012, **134**, 2028–2031.
22 D. McDowall, M. Walker, M. Vassalli, M. Cantini, N. Khunti, C. J. C. Edwards-Gayle, N. Cowieson and D. J. Adams, *Chem. Commun.*, 2021, **57**, 8782–8785.
23 Y. Fang, J. Shi, J. Liang, D. Ma and H. Wang, *Nat. Commun.*, 2025, **16**, 1058.
24 E. J. Berns, S. Sur, L. Pan, J. E. Goldberger, S. Suresh, S. Zhang, J. A. Kessler and S. I. Stupp, *Biomaterials*, 2014, **35**, 185–195.
25 A. C. Farsheed, C. Zevallos-Delgado, L. T. Yu, S. Saeidifard, J. W. R. Swain, J. T. Makhoul, A. J. Thomas, C. C. Cole, E. G. Huitron, K. J. Grande-Allen, M. Singh, K. V. Larin and J. D. Hartgerink, *ACS Nano*, 2024, **18**, 12477–12488.
26 E. Sleep, B. D. Cosgrove, M. T. McClendon, A. T. Preslar, C. H. Chen, M. H. Sangji, C. M. R. Pérez, R. D. Haynes, T. J. Meade, H. M. Blau and S. I. Stupp, *Proc. Natl. Acad. Sci. U. S. A.*, 2017, **114**, E7919–E7928.
27 A. S. Loch, I. Mikhail, S. Bianco, D. Ghosh, R. R. Sonani, V. Chechik, M. Vassalli, E. H. Egelman, A. J. Smith and D. J. Adams, *ACS Appl. Mater. Interfaces*, 2025, **17**, 30297–30305.
28 H. Li, Z. Zhao, M. Yang, Y. Peng, Z. Du and F. Sun, *Cell Rep. Phys. Sci.*, 2024, **5**, 102137.
29 S. de Mulatier, M. Nasreldin, R. Delattre, M. Ramuz and T. Djenizian, *Adv. Mater. Technol.*, 2018, **3**, 1700320.
30 K. E. Horner, M. A. Miller, J. W. Steed and P. M. Sutcliffe, *Chem. Soc. Rev.*, 2016, **45**, 6432–6448.
31 J. A. Lee, N. Li, C. S. Haines, K. J. Kim, X. Lepró, R. Ovalle-Robles, S. J. Kim and R. H. Baughman, *Adv. Mater.*, 2017, **29**, 1700870.
32 L. Schefer, J. Adamcik, M. Diener and R. Mezzenga, *Nanoscale*, 2015, **7**, 16182–16188.
33 R. Freeman, M. Han, Z. Álvarez, J. A. Lewis, J. R. Wester, N. Stephanopoulos, M. T. McClendon, C. Lynsky, J. M. Godbe, H. Sangji, E. Luijten and S. I. Stupp, *Science*, 2018, **362**, 808–813.
34 C. Tangsombun and D. K. Smith, *J. Am. Chem. Soc.*, 2023, **145**, 24061–24070.
35 G. Liu, Z. Ding, Q. Yuan, H. Xie and Z. Gu, *Front. Chem.*, 2018, **6**, 439.
36 M. T. I. Mredha, H. H. Le, P. Trtik, J. Cui and I. Jeon, *Mater. Horiz.*, 2019, **6**, 1504–1511.
37 X. Zhang, Z. Lou, X. Yang, Q. Chen, K. Chen, C. Feng, J. Qi, Y. Luo and D. Zhang, *ACS Appl. Polym. Mater.*, 2021, **3**, 5039–5050.
38 M. D. Lima, N. Li, M. J. de Andrade, S. Fang, J. Oh, G. M. Spinks, M. E. Kozlov, C. S. Haines, D. Suh, J. Foroughi, S. J. Kim, Y. Chen, T. Ware, M. K. Shin, L. D. Machado, A. F. Fonseca, J. D. Madden, W. E. Voit, D. S. Galvão and R. H. Baughman, *Science*, 2012, **338**, 928–932.
39 P. Chen, Y. Xu, S. He, X. Sun, S. Pan, J. Deng, D. Chen and H. Peng, *Nat. Nanotechnol.*, 2015, **10**, 1077–1083.
40 S. Fleming and R. V. Ulijn, *Chem. Soc. Rev.*, 2014, **43**, 8150–8177.
41 D. Ghosh, S. M. Coulter, G. Laverty, C. Holland, J. J. Doutch, M. Vassalli and D. J. Adams, *Biomacromolecules*, 2024, **25**, 3169–3177.
42 F. Kun, L. Allan, A. Batool, Z. Danku and G. Pál, *Phys. Rev. Res.*, 2024, **6**, 033344.
43 X. Zhou, S. Fang, X. Leng, Z. Liu and R. H. Baughman, *Acc. Chem. Res.*, 2021, **54**, 2624–2636.
44 H. Liu, C. Wang, J. Tan, W. Yang and L. Cheng, *Comput. Mater. Sci.*, 2021, **194**, 110463.

45 V. Negi, A. Sengab and R. C. Picu, *J. Mech. Behav. Biomed. Mater.*, 2019, **94**, 1–9.
46 Y. Rao and R. J. Farris, *J. Appl. Polym. Sci.*, 2000, **77**, 1938–1949.
47 N. Pan, *J. Mater. Sci.*, 1993, **28**, 6107–6114.
48 P. K. Porwal, I. J. Beyerlein and S. L. Phoenix, *J. Mech. Mater. Struct.*, 2006, **1**, 1425–1447.
49 S. Kostic, V. Kocovic, S. P. Savic, D. Miljanic, J. Miljojkovic, M. Djordjevic and D. Vukelic, *Appl. Sci.*, 2024, **14**, 3046.
50 Z. Guo, Z. Shan, J. H. Huang, D. Wang, H. Huang and Z. Chen, *Text. Res. J.*, 2022, **92**, 4933–4953.
51 X. Teng, D. Shi, X. Jing, S. Lyu and X. Yang, *Chin. J. Aeronaut.*, 2021, **34**, 278–288.
52 Z. Yang, Available at SSRN 5035268, 2024, **https://papers.ssrn.com/sol3/papers.cfm?abstract_id=5035268**.
53 Y.-L. Zhao and J. F. Stoddart, *Langmuir*, 2009, **25**, 8442–8446.
54 S. Panja and D. J. Adams, *Chem. Soc. Rev.*, 2021, **50**, 5165–5200.
55 C. A. Schneider, W. S. Rasband and K. W. Eliceiri, *Nat. Methods*, 2012, **9**, 671–675.
56 O. Arnold, J. C. Bilheux, J. M. Borreguero, A. Buts, S. I. Campbell, L. Chapon, M. Doucet, N. Draper, R. F. Leal, M. A. Gigg, V. E. Lynch, A. Markvardsen, D. J. Mikkelson, R. L. Mikkelson, R. Miller, K. Palmen, P. Parker, G. Passos, T. G. Perring, P. F. Peterson, S. Ren, M. A. Reuter, A. T. Savici, J. W. Taylor, R. J. Taylor, R. Tolchenov, W. Zhou and J. Zikovsky, *Nucl. Instrum. Methods Phys. Res., Sect. A*, 2014, **764**, 156–166.
57 SasView – Small Angle Scattering Analysis, **https://www.sasview.org/** (accessed 2025-06-16).